JOURNAL OF APPLIED ELECTROCHEMISTRY 10 (1980) 251–260

Thermal battery cells utilizing molten nitrates as the electrolyte and oxidizer

M. H. MILES, A. N. FLETCHER

Chemistry Division, Naval Weapons Center, China Lake, California 93555, USA

Received 4 April 1979

The $Ca/LiNO_3$–LiCl–KCl (50–25–25 mol%) thermal battery cell can be activated at 160° C and operated over a temperature range of 250–450° C to produce 2.5–2.8 V at open-circuit and initial operating voltages above 2 V at 10 mA cm^{-2}. At operating temperatures between 250 and 350° C, this system shows promise for applications requiring a sixty-minute thermal battery. Cell lifetimes decrease at higher temperatures due to the accelerating reaction of calcium with the molten nitrate salt to form gaseous products. An experimental energy density value of 142 W h kg^{-1} was obtained at 300° C during constant current discharge at 10 mA cm^{-2}. Effects of applied face pressure on cell discharge characteristics were small. At current densities above 20–30 mA cm^{-2}, the cell performance deteriorates due to polarization at the anode. This is probably caused by the precipitation of CaO which blocks the active sites at the anode.

1. Introduction

Thermal battery cells contain an electrolyte that is solid and non-conductive at normal temperatures but becomes ionically conductive when a built-in pyrotechnic heat source activates the battery by melting the solid electrolyte. These characteristics make thermal batteries capable of essentially unlimited storage life and of rapid and reliable activation. Thermal batteries can be designed to withstand severe shock and vibrations; therefore they can fulfil many military, aerospace, and emergency applications [1–5].

Most of the thermal batteries presently employed in missile systems make use of a LiCl–KCl mixture as the electrolyte, calcium metal as the anode, and $CaCrO_4$ as the cathodic material. The relatively high melting point of the electrolyte limits activation of the battery to temperatures above 352° C. A complex series of chemical and electrochemical reactions occur at the anode to form a liquid calcium–lithium alloy, a KCl–$CaCl_2$ double salt (m.p. = 752° C) and a Ca_2CrO_4Cl layer adjacent to the anode [6, 7]. Due to these complex interactions, thermal batteries using LiCl–KCl mixtures are generally designed to operate at internal temperatures between 475 and 550° C [6–8]. At higher temperatures, the self-discharge reaction of calcium with $CaCrO_4$ accelerates leading to a thermal runaway [7].

Nitrate salts are attractive for use in thermal batteries because of their low melting points. For example, KNO_3–$LiNO_3$ mixtures melt at temperatures as low as 132° C [9]. The use of a lower melting electrolyte can shorten a battery's activation time and reduce the weight of heat sources and insulation. Another major advantage is that the molten nitrate can also function as the oxidizer thus simplifying battery construction by eliminating the necessity for the addition of a separate oxidizer such as $CaCrO_4$. Furthermore, nitrate salts are low-hazard materials, unlike chromates, which are recognized as health hazards ($CaCrO_4$ has been designated as a carcinogen and is on OSHA's recent list of confirmed carcinogens)[10, 11]. A separate study of the calcium anode in molten nitrates as well as a study of the nitrate cathode have been reported previously [12, 13]. These half-cell studies showed that the use of $LiNO_3$ aids the cathodic reaction while added halide salts improve the anode by attacking the protective oxide film. Therefore, thermal battery cell tests were made using various salt mixtures containing $LiNO_3$ and added halides.

0021–891X/80/020251–10$03.00/0

2. Experimental

Single cell discharge experiments were conducted in a stainless steel test chamber under a helium-filled inert atmosphere. The main features of the bottom portion of the single cell test set-up are shown in Fig. 1. The top portion of the test chamber consisted primarily of a Swagelock T-joint connected through a reducer to the inner steel tube and providing also for connection to a vacuum/helium line. Face pressure on the electrochemical cell was maintained by the compression of the stainless steel spring (Associated Spring Corp.). Using the force constant for the spring (1240 kg s^{-2}), the calculated face (axial) pressure was usually about 4.3×10^5 Pa (4.2 atm).

The electrochemical cells were fabricated from calcium discs (ROC/RIC, 99%) 1.25 mm thick and 6.35 mm in diameter (0.317 cm^2), spot-welded to a Ca/Fe bi-metallic disc of the same diameter but only 0.3 mm in thickness. The aluminium lead wire was then spot-welded to the Fe side of the bi-metal. Two fibreglass filter paper discs (Gelman, type A, 0.3 mm thickness) containing the electrolyte were fused to the mechanically cleaned calcium surface by using a spot heater lamp. The back side and edges of the bi-metallic disc were masked off by applying a thin layer of Sauereisen cement (no. 1) and then drying by use of a heat gun after the soapstone spacers were in place. After connecting the top and bottom portions of the test chamber, the aluminium lead wire emerging from the top was sealed with wax.

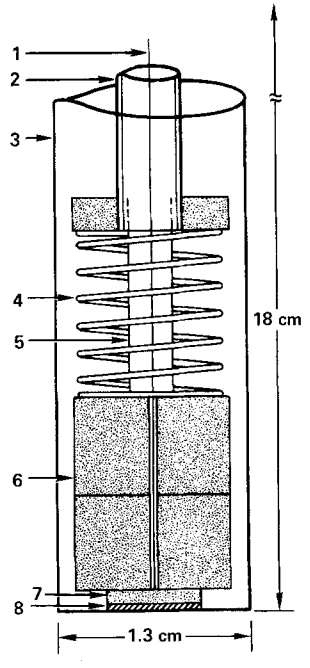

Fig. 1. Side view of the bottom portion of the single-cell test set-up. 1, anode lead; 2, inner stainless steel tube containing insulating glass tubing and connected to the top portion of the test chamber; 3, outer stainless steel tube; 4, stainless steel spring; 5, insulating glass tubing; 6, soapstone spacers; 7, calcium anode; 8, fibreglass disc containing the oxidizing electrolyte.

The test chamber containing the assembled cell was then connected to the vacuum/helium line and re-filled with helium several times before finally evacuating several hours to about 10^{-7} atm to remove any moisture. Prior to activation, the test chamber was re-filled with helium to give a gas pressure of 1 atm at room temperature.

The electrochemical cell was activated by suddenly immersing the bottom portion of the test chamber into a fluidized sand bath (Tecam) maintained at the desired experimental temperature. The bath temperature was measured with a digital thermocouple thermometer (Fluke, Model 2165A) as well as with a dial thermometer and was generally controlled to within ±3° C during an experimental run. Cell discharge was initiated when the cell voltage had stabilized 2–3 min after activation. Constant current discharge was maintained by a Keithley current source (Model 225). Attempts to maintain constant current discharge by using a PAR Model 173 potentiostat/galvanostat (Princeton Applied Research Corp.) gave an error of about ±2 mA on all current settings whenever the cell was grounded. In our cell test set-up, the cell was grounded through the vacuum line connection as well as through the recorders used.

During cell activation and discharge, the cell voltage, cell resistance, and the gas pressure in the test chamber were continually recorded using a strip chart recorder (HP 7100B) and digital recorder (HP H24562A). The cell resistance was measured by the use of a Hewlett-Packard milliohmmeter (Model 4328A) that gives accurate readings even when in contact with a d.c. circuit. The gas pressure in the test chamber was monitored by the use of a transducer (Pace, Model CD25).

In order to measure the polarization occurring at the anode and cathode separately, similar single cell tests were conducted using an open nickel lid placed on a hot plate [13]. A metal rod was used with a spring and soapstone spacers to maintain

face pressure on the cell. An L-shaped reference electrode containing 0.1 m $AgNO_3$ in equimolar KNO_3–$NaNO_3$ was used to monitor the potential of the cathode. The PAR instrument was used for potential measurements versus the reference electrode while the Keithley instrument again provided the constant current.

The electrochemical cells, on average, contained about 65 mg of calcium, 25 mg of the electrolyte salt and 4 mg of the fibreglass filter paper. Based upon electrochemical equivalents, the calcium was present in excess. After each experiment, the amount of calcium remaining was determined by reacting it with water and measuring the volume of hydrogen gas evolved.

3. Results

Single cell tests were made using various salt mixtures containing $LiNO_3$ and added halides. The most promising results were obtained using a 50–25–25 mole per cent (mol%) mixture of $LiNO_3$–LiCl–KCl. This mixture was actually prepared as the equivalent formulation of $LiNO_3$–LiCl–KNO_3 (25–50–25 mol%, m.p. = 160° C). Fig. 2 shows cell discharge results for this mixture at a constant current density of 10 mA cm^{-2} at temperatures of 250, 300, 350, and 400° C. A cell test at 450° C gave results similar to those obtained at 400° C, hence this system is operable over a temperature range of 250–450° C to produce 2.5–2.8 V at open-circuit and inital operating voltages above 2 V at 10 mA cm^{-2}. Activated lifetimes to 75% of the peak discharge voltages were 45, 26, 21, 10, and 9 min at temperatures of 250, 300, 350, 400, and 450° C, respectively. This cell could also be activated at lower temperatures, but cell performance was poor (1.2 V at 2 mA cm^{-2} at 175° C).

For these same cell tests, the cell resistance during cell discharge at 10 mA cm^{-2} is illustrated in Fig. 3. At the lower temperatures, the cell resistance shows only gradual changes with time. At 400° C, the cell resistance increased much more rapidly with time and exceeded the limit of the milliohmmeter (100 Ω) by the time the cell voltage dropped to zero. The decrease in cell voltage due to the *IR* effect accounts for only a small part of the total cell polarization. Even with a cell resistance of 100 Ω, the ohmic polarization at 10 mA cm^{-2} would only be 0.317 V out of a total cell poarization exceeding 2 V.

At operating temperature below 400° C, the Ca/$LiNO_3$–LiCl–KCl cell shows promise for applications requiring a sixty-minute thermal battery.

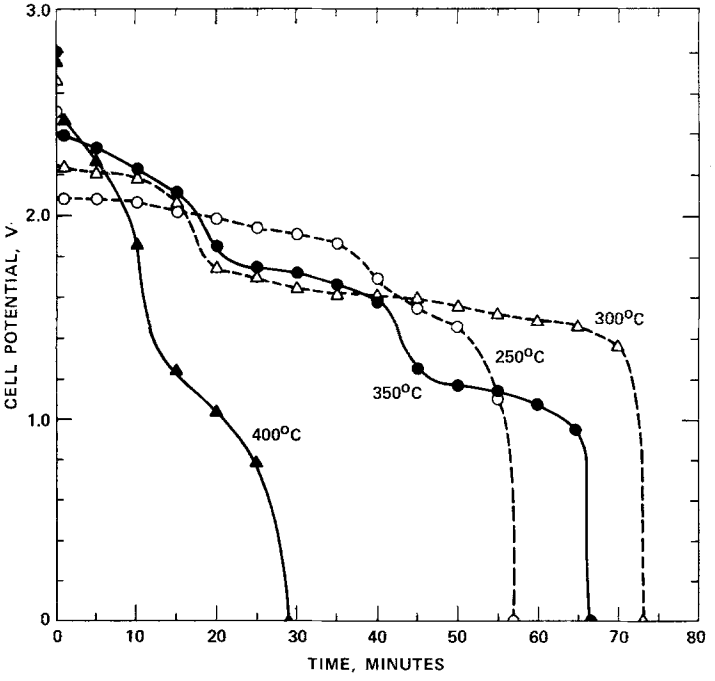

Fig. 2. Cell potentials during discharge at a constant current density of 10 mA cm^{-2} at 250, 300, 350, and 400° C.

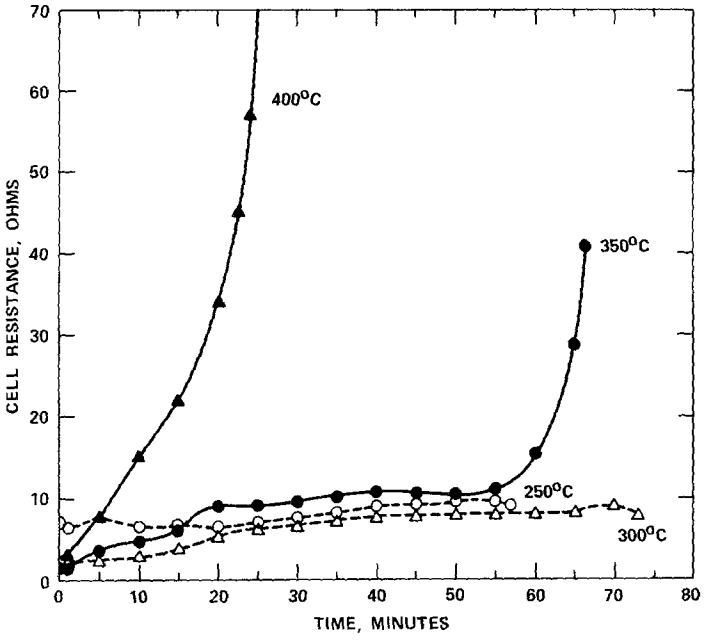

Fig. 3. Cell resistances during cell discharge at 10 mA cm^{-2} at 250, 300, 350 and 400° C.

In Fig. 2, the cell lifetimes to zero voltage at 250, 300, and 350° C are 57, 73, and 66 min, respectively. Cell voltages remained above 1.5 V for over 40 min in each of these tests. The much lower operating temperature range of this system compared with conventional thermal batteries (500–600° C) is a distinct advantage for applications requiring long activated lifetimes [14–16]. Activated lifetimes, however, become considerably shorter at temperatures above 350° C or at current densities above about 20–30 mA cm^{-2}.

Fig. 4 illustrates the effect of the current density upon the cell potential at 250, 300, and 350° C. The potentials were generally recorded after 30–120 s of cell discharge at each current density. Cell potentials were usually fairly steady except at current densities above about 20–30 mA cm^{-2} where the potential would decrease steadily with time. At even higher current densities, the cell potential would decrease rapidly to zero, but the cell would recover within 1–2 min at open-circuit and could still sustain the passage of lower current densities. Cell potential versus current density studies at temperatures higher than 350° C

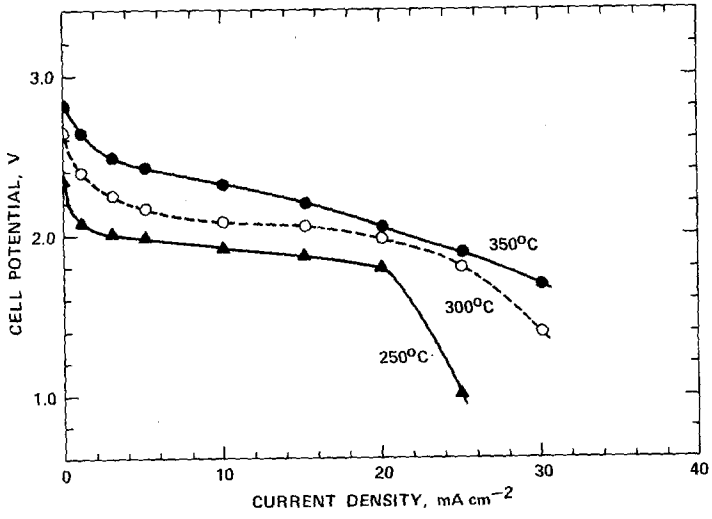

Fig. 4. Effect of current density upon the cell potential at 250, 300, and 350° C.

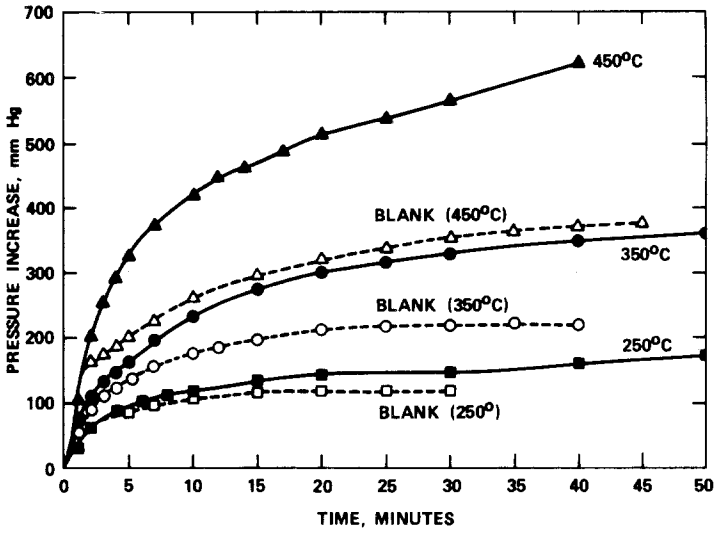

Fig. 5. Increase in gas pressure within the test chamber with time for activated cells and blanks at 250, 350, and 450° C.

were complicated by the more rapid decrease in cell potential and increase in cell resistance (see Figs. 2 and 3).

A disadvantage of nitrate systems for thermal batteries is the fact that gas can form from corrosion and decomposition reactions at high cell temperatures [1]. Fig. 5 shows the increase in gas pressure within the test chamber upon immersing the bottom portion in the sand bath. The major part of the pressure increase results from the heating of the helium gas initially present in the chamber at 760 mm Hg (1 atm) at room temperature. Tests of blank cells containing no nitrates (dashed lines, Fig. 5) show this heating effect. The difference between the cell test and the blank at a given temperature should represent the actual formation of gaseous products from reactions involving nitrates. The free volume of the test chamber is estimated to be about 25 cm^3, however more than half of this is above the sand bath, therefore an estimate of the mean temperature would be required in calculating the number of moles of gas produced. By measuring the pressure of the cell at room temperature after the test, the moles of gaseous products are calculated to be 0.7×10^{-4}, 2×10^{-4}, and 4×10^{-4} moles for the experiments at 250, 350, and 450° C shown in Fig. 4. Calculations based upon pressures shown in Fig. 5 and the average of the bath and room temperatures gives about half as many moles of gaseous products. These calculations suggest that at high temperatures there may be a total of about one mole of gaseous products per mole of $LiNO_3$ initially present, hence provisions for venting will be required for these thermal battery cells. Single cell tests have shown that the sudden venting of gaseous products or even rapid cell evacuation and the admission of air have very little effect on cell discharge characteristics.

Fig. 6 shows the results of a typical 'open-pan' cell study at 10 mA cm^{-2} at 350° C where a Ag^+/Ag reference electrode was introduced to measure the potential of the cathodic reaction. The potential of the anodic reaction could then be calculated from the relationship

$$E_{\text{anode}} = E_{\text{cathode}} - E_{\text{cell}}.$$

Both the anodic and cathodic potentials are actually negative in sign to the Ag^+/Ag reference electrode. During the first 75 min of cell discharge, the potential of the anode was relatively constant (− 2.70 to − 2.85 V versus Ag^+/Ag) while the potential of the cathode varied from − 0.45 V to about − 1.0 V. Towards the end of the cell lifetime, both the anode and cathode showed significant changes in potential, but the major portion of the polarization still occurred at the cathode.

These 'open-pan' studies generally gave longer activated lifetimes than the experiments in the closed test chamber. The presence of air or moisture does not appear to be the major factor since studies conducted with the test chamber open to the atmosphere gave results similar to those obtained in the helium atmosphere. Another

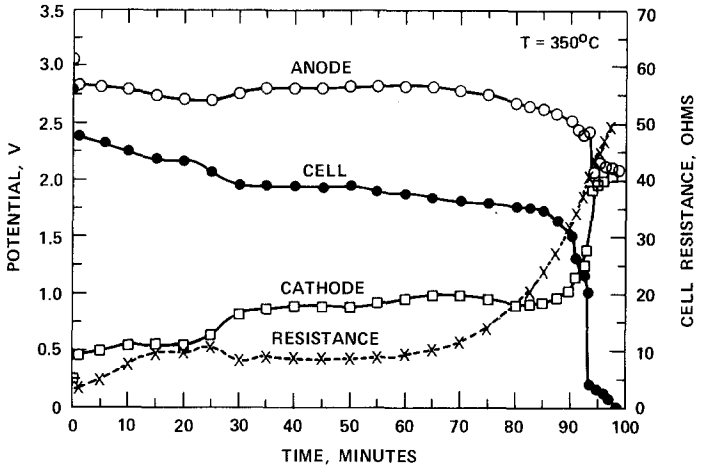

Fig. 6. Open-pan cell discharge at 10 mA cm^{-2} at 350° C showing anode, cathode, and cell potentials with time as well as the cell resistance with time.

experimental difference, however, is the fact that the cathodic reaction occurs on a nickel surface in 'open-pan' tests and on a stainless steel surface in the test chamber.

The effect of the current density upon the anodic, cathodic and cell potential in 'open-pan' tests at 350° C is shown in Fig. 7. The potentials were generally measured within 30–120 s at each current density as in the similar studies in the test chamber (Fig. 4). This experiment shows that the cell polarization at high current densities is due to polarization of the anode. The results in Fig. 7 suggest linear Tafel behaviour for the anodic and cathodic reaction at current densities between about 2 and 20 mA cm^{-2}.

Several cell tests were conducted in which the initial face pressure exerted on the cell varied from about 0.4×10^5 Pa to about 6×10^5 Pa. Any effects of the face pressure on the cell discharge characteristics were smaller than normal experimental variations. In 'open-pan' studies, however, the face pressure could be varied directly during cell discharge. Increasing the face pressure produced slightly more favourable cell potentials while reducing the face pressure gave slightly less favourable potentials. The observed variations were generally within ± 0.1 V and reflected potential changes at the anode. Changes in the face pressure seemed to have no effect on the open-circuit cell voltage. Similar results have been reported for anode–cathode contact pressure experiments involving a filmed lithium anode [17].

Table 1 gives the results for the determination of the calcium metal remaining after cell discharge

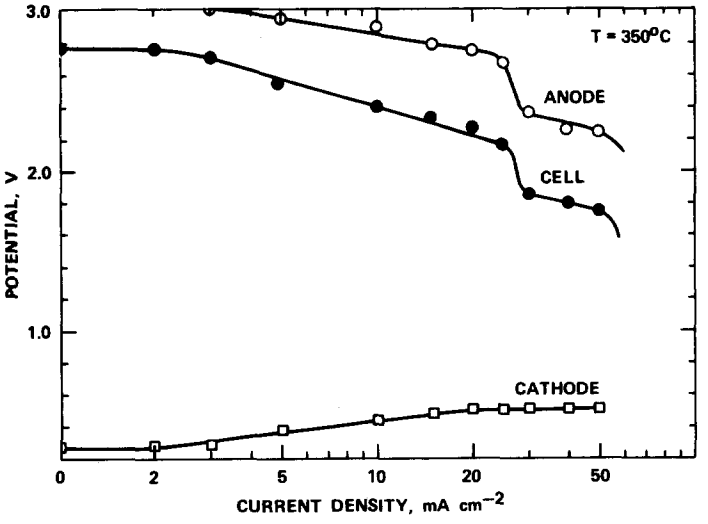

Fig. 7. Effect of current density upon the anodic, cathodic, and cell potentials in an open-pan test at 350° C.

Table 1. Calcium metal remaining in cells discharged to 0 V at 10 mA cm^{-2} in the helium-filled test chamber. The initial weight of calcium metal was about 65 mg

Cell discharge temperature (° C)	*Calcium metal* (mg)
250	62
300	47
350	35
400	22
450	13

to 0 V at 10 mA cm^{-2}. Similar results were obtained for the 'open-pan' studies. Like the cell resistance (Fig. 3) and the cell pressure increase (Fig. 5), the results in Table 1 are strongly temperature dependent. These results suggest that at the lower temperatures, much smaller amounts of calcium metal could be used without affecting the cell performance.

Other mixtures tested containing $LiNO_3$ and added halide included 70–25–5, 55–25–20, and 50–25–25 mol% mixtures of $LiNO_3$–KNO_3–LiCl as well as 65–25–10 and 20–40–40 mol% mixtures of $LiNO_3$–LiCl–KCl. A 50–50 mol% mixture of $LiNO_3$–LiCl and a 40–20–20–20 mol% mixture of $LiNO_3$–LiCl–KCl–$CaCrO_4$ were also tested. Mixtures containing lower chloride content generally gave lower cell voltages, a more rapid increase in cell resistances, and shorter lifetimes than the 50–25–25 mol% mixture of $LiNO_3$–LiCl–KCl. The 20–40–40 mol% mixture of $LiNO_3$–LiCl–KCl gave good cell performance at 350° C, but its relatively high melting point (~ 280° C) would limit its lower temperature range.

An electrolyte consisting of both solid and liquid phases over a wide temperature range tends to improve the performance of thermal battery cells [1]. For example, $LiNO_3$–LiCl–KCl (50–25–25 mol%) begins to melt at about 160° C, yet undissolved crystals remain even at 360° C. Undissolved chloride salts probably restrict the transport of nitrate to the calcium, thus reducing the rate of direct reaction. This mixture also forms a solid solution that seems to co-exist with the liquid and undissolved crystals over a wide temperature range.

A cell test of $LiNO_3$–LiBr–KBr (50–25–25 mol%, m.p. ~ 200° C) at 350° C gave similar results to the corresponding chloride system. Upon melting, this bromide system develops a yellow coloration suggesting a reaction with nitrates to produce bromine. A preparation of $LiNO_3$–LiI–KI (50–25–25 mol%) produced, upon melting, a dark brownish-red colour and violet iodine fumes to the extent that it could not be used. An 'open-pan' cell test of $LiNO_3$–LiCl–$K_2Cr_2O_7$ (50–25–25 mol%, m.p. ~ 160° C) at 350° C gave good cathode potentials (+ 0.2 V versus Ag^+/Ag) but the anode polarized badly even at low current densities. The rapid onset of a high cell resistance exceeding 100 Ω suggests the decomposition of the $K_2Cr_2O_7$ to form an insoluble, non-conducting product at the anode.

For comparison with the nitrate systems, an 'open-pan' test of calcium with LiCl–KCl–$CaCrO_4$ (47–34–19 mol%, m.p. ~ 340° C) was made at 425° C. This cell gave 2.61 V at open-circuit and 2.53 V, 2.41 V, and 2.21 V for 30–120 s at current densities of 10, 20, and 30 mA cm^{-2}, respectively. At current densities above 30 mA cm^{-2}, the cell performance deteriorates due to serious polarization at the anode. This could be due to the build-up of low mobility reaction products such as $KCl \cdot CaCl_2$ at the anode interface [6, 7]. Although it is possible that KCl–$CaCl_2$ may also form at the anode in the $LiNO_3$–LiCl–KCl systems, ideal solubility calculations suggest that the much less soluble CaO would form instead. In support of this, a potassium-free mixture of $LiNO_3$–LiCl (50–50 mol%, m.p. = 227° C) performed similarly to the $LiNO_3$–LiCl–KCl mixture at 350° C.

During these experiments, it was observed that molten salt mixtures containing $CaCrO_4$ would dissolve the fibreglass disc and attack glass beakers. The LiCl–KCl–$CaCrO_4$ mixture as well as $LiNO_3$–LiCl–KCl–$CaCrO_4$ (40–20–20–20 mol%, m.p. ~ 210° C) showed this agressive action towards glass while $LiNO_3$–LiCl–$K_2Cr_2O_7$ did not. This suggests that the following reaction

$$2\ CrO_4^{2-} + SiO_2 \rightleftharpoons Cr_2O_7^{2-} + SiO_3^{2-} \qquad (1)$$

should be considered in thermal battery cells containing both chromates and silica.

4. Discussion

Thermodynamic calculations for the cell reaction

$$Ca_{(s)} + LiNO_{3(l)} \rightarrow CaO_{(s)} + LiNO_{2(l)} \qquad (2)$$

at 350° C yields a standard cell potential (E^0) of

2.81 V. This value is in good agreement with the experimental open-circuit potentials observed. The theoretical energy density of this cell is, therefore, 1380 W h kg^{-1}. The experimental energy density at 350° C was 60 W h kg^{-1} for the study in the closed test chamber (Fig. 2) and 100 W h kg^{-1} for the 'open-pan' study (Fig. 6). Based upon the weight of $LiNO_3$ used (~ 13 mg), the current efficiency for the test shown in Fig. 6 was 51%. In a few tests designed to maximize the energy density at 10 mA cm^{-2}, an experimental value of 142 W h kg^{-1} was obtained at 300° C using 14 mg of calcium and 25 mg of the $LiNO_3$–LiCl–KCl (50–25–25 mol%) electrolyte. The energy density up to 75% of the peak voltage yields a slightly lower value of 131 W h kg^{-1}.

The sudden increase in cell polarization at high current densities is due mainly to the polarization of the anode (see Figs. 4 and 7). This is likely caused by the precipitation of CaO which blocks the active sites operating across the protective film. Similar behaviour has been reported for a filmed lithium anode when the current density exceeds the critical level [18]. Cell recovery within 1–2 min at open-circuit would result from the dissolution of the blocking material or the formation of new active sites on the anode. In a previous study of the calcium anode [12], current densities as high as 100 mA cm^{-2} could be passed without causing critical polarization. In those half-cell studies, however, the anode was suspended in a large excess of electrolyte such that any precipitate formed adjacent to the electrode surface would tend to settle in the solution. In the cell tests reported here, cell products are confined to the thin filter paper discs containing the electrolyte.

Oxide precipitation at the cathode did not appear to be a major cause of polarization for the cell arrangement and electrolyte composition used in these experiments. Since cyclic voltammetric experiments in progress indicate that CaO is less soluble than Li_2O, it seems reasonable that oxide precipitation would first affect the anode, especially considering that the active surface at the anode probably consists of breaks in the oxide film. The cathode, on the other hand, develops a high surface roughness factor due to the attack on the metal by the electrolyte. The unusually strong corrosive action of the $LiNO_3$–LiCl–KCl (50–25–25 mol%) mixture on the nickel pan used in preparing the electrolyte discs made it necessary to use a platinum pan instead. During cell tests, dark spots always formed where the electrolyte disc contacted the cathode surface. Cyclic voltammetric studies on nickel electrodes show that the formation of nickel oxide increases the active surface area by about a factor of ten. The spread of excess electrolyte on the cathode surface would also tend to increase the actual surface area of the cathode.

The gradual depletion of $LiNO_3$ is the likely cause of the polarization at the cathode during constant current experiments (Fig. 6). The nitrate is consumed by the direct reaction with calcium as well as by electrochemical reduction. Cell life becomes considerably shorter at temperatures above 350° C due to the increasing rate of the self-discharge reaction. This is consistent with differential scanning calorimetry (DSC) studies of calcium in nitrate salts containing added halides that generally show exothermic peaks between 350–400° C [12]. DSC studies of the Ca/$LiNO_3$–LiCl–KCl (50–25–25 mol%) system show a melting endothermic peak at about 160° C and several very strong exothermic peaks beginning at about 350° C.

The linear Tafel regions in Fig. 7 yield experimental transfer coefficients of $\alpha_a = 0.37$ and $\alpha_c = 0.52$ for the anodic and cathodic reactions. The cathodic transfer coefficient is in reasonable agreement with previous studies of nitrate reduction [13]. The relatively constant cathodic potential at current densities above 20 mA cm^{-2} may reflect changes in the effective surface area as discussed above. The dual barrier model proposed by Meyer [19, 20] could be applied to the anodic reaction involving the calcium oxide film to explain the low transfer coefficient, however, experimental results are not very consistent since the active surface area of the anode cannot be readily controlled.

Cell resistance calculated from

$$R = lA^{-1}k^{-1}$$

using the electrolyte layer thickness (l), cell area (A), and the specific conductivity (k) of molten $LiNO_3$ [21] yields values of less than 0.2 Ω. Measured cell resistances were always at least a factor of ten larger than this, suggesting that the oxide film at the anode makes a sizeable contribution to the total cell resistance.

The results of cell potential, E_{cell}, versus current density, i, shown in Fig. 4, can be represented theoretically by the equation

$$E_{cell} = E_{rev} - |\eta_a| - |\eta_c| - i\bar{R} \quad (3)$$

where E_{rev} is the thermodynamic reversible potential for the cell and η_a and η_c are the anodic and cathodic overvoltages. The resistance, $\bar{R}$, is defined by

$$\bar{R} = A \sum R_j \quad (4)$$

where A is the cell area and ΣR_j is the sum of all internal resistances. At high overvoltages, η_a and η_c may be expressed by the Tafel equations

$$\eta_a = a_a + b_a \ln i \quad (5)$$

$$|\eta_c| = |a_c| + |b_c| \ln i \quad (6)$$

and substituted into Equation 3 to give

$$E_{cell} = E_{rev} - (a_a + |a_c|) - (b_a + |b_c|) \ln i - i\bar{R}. \quad (7)$$

The change in cell potential with current density at constant temperature and resistance

$$\left(\frac{\partial E_{cell}}{\partial i}\right)_{T,\bar{R}} = -\frac{b_a + |b_c|}{i} - \bar{R} \quad (8)$$

can be used in interpreting the results shown in Fig. 4. Calculations based upon the measured cell resistances and Tafel slopes show that the first term will dominate for the current range used in these experiments. The slope of E_{cell} versus i should, therefore, become less negative with increasing current density and should eventually approach a limiting value of $\bar{R}$. The experimental results in Fig. 4 show the expected trends up to current densities of about 20 mA cm^{-2}. The departure from the theoretical behaviour at higher current densities reflect the sudden changes in the Tafel parameters for the anodic reaction (Fig. 7) as the reactive sites become blocked by calcium oxide.

For low overvoltages

$$\eta = \frac{RT}{zF}\frac{i}{i_0} \quad (9)$$

where R is the gas constant, F is the Faraday constant, z is the number of electrons transferred in the rate-determining step, and i_0 is the exchange current density. Substituting this expression for the anodic and cathodic overvoltages in Equation 3 and differentiating gives

$$\left(\frac{\partial E_{cell}}{\partial i}\right)_{T,\bar{R}} = -\frac{RT}{F}\left(\frac{1}{z_a i_{0,a}} + \frac{1}{z_c i_{0,c}}\right) - \bar{R} \quad (10)$$

showing that the initial slope at low overvoltages is independent of the current density but varies with the anodic and cathodic exchange current densities, $i_{0,a}$ and $i_{0,c}$. This equation can be used to estimate the exchange current density of the slowest electrode reaction and yields $i_0 = 10^{-5}$ A cm^{-2} at 250° C and $i_0 = 10^{-4}$ A cm^{-2} at 350° C for the experiments shown in Fig. 4. This is in good agreement with previously reported i_0 values for the reduction of $LiNO_3$ [13].

References

[1] C. W. Jennings, in 'The Primary Battery,' Vol. II (edited by N. C. Cahoon and G. W. Heise), John Wiley, New York (1976) pp. 263–93.

[2] J. C. Nardi, J. K. Erbacher, C. L. Hussey and L. A. King, *J. Power Sources* **3** (1978) 81.

[3] F. Smith and D. R. Cottingham, in *Twenty-Seventh Power Sources Symposium*, PSC Publications Committee, Red Bank, N.J. (1976) pp. 155–58.

[4] B. H. Van Domelen and R. D. Wehrle, in *Ninth Intersociety Energy Conversion Engineering Conference Proceedings*, American Society of Mechanical Engineers, New York (1974) pp. 665–70.

[5] K. R. Grothaus, in *Twenty-Sixth Power Sources Symposium*, PSC Publications Committee, Red Bank, N.J. (1974) pp. 141–44.

[6] D. A. Nissen, *J. Electrochem. Soc.* **126** (1979) 176.

[7] F. Tepper, in *Ninth Intersociety Energy Conversion Engineering Conference Proceedings*, American Society of Mechanical Engineers, New York (1974) pp. 671–77.

[8] D. M. Bush, in *Twenty-Sixth Power Sources Symposium*, PSC Publications Committee, Red Bank N.J. (1974) pp. 144–47.

[9] D. H. Kerridge, in 'Inorganic Chemistry: Main Group Elements, Groups V and VI,' (edited by C. C. Addison and D. B. Sowerby) Series 1, Vol. 2, Butterworths, London (1972) pp. 30–60.

[10] W. S. Bishop and A. A. Benderly, in *Twenty-Seventh Power Sources Symposium*, PSC Publications Committee, Red Bank, N.J. (1976) pp. 158–60.

[11] *Chem. Eng. News* **56** 31 July (1978) 20.

[12] M. H. Miles, D. A. Fine and A. N. Fletcher, *J. Electrochem. Soc.* **125** (1978) 1209.

[13] A. N. Fletcher, M. H. Miles and M. L. Chan, *J. Electrochem. Soc.* **126** (1979) 1496.

[14] G. C. Bowser and C. L. Paxton, in *Ninth Intersociety Energy Conversion Engineering Con-*

ference Proceedings, American Society of Mechanical Engineers, New York (1974) pp. 684–87.

[15] A. Baldwin, in *Twenty-Seventh Power Sources Symposium*, PSC Publications Committee, Red Bank N.J. (1976) pp. 152–54.

[16] D. Bush and A. Baldwin, in 'Power Sources, 6. Research and Development in Non-Mechanical Electrical Power Sources,' Academic Press, New York (1977) pp. 581–94.

[17] E. L. Littauer, K. C. Tsai and R. P. Hollandsworth, *J. Electrochem. Soc.* **125** (1978) 845.

[18] E. L. Littauer and K. C. Tsai, *J. Electrochem. Soc.* **123** (1976) 964.

[19] R. E. Meyer, *ibid* **107** (1960) 847.

[20] M. H. Miles, E. A. Klaus, B. P. Gunn, J. R. Locker and W. E. Serafin, *Electrochim. Acta* **23** (1978) 521.

[21] G. J. Janz, 'Molten Salts Handbook,' Academic Press, New York, (1967) pp. 290–97.